

X-FEM modeling of large plasticity deformation; a convergence study on various blending strategies for weak discontinuities

A. R. Khoei, M. Vahab, H. Ehsani and M. Rafieerad

Department of Civil Engineering, Center of Excellence in Structures and Earthquake Engineering, Sharif University of Technology, Tehran, Iran

ABSTRACT

In the extended finite element method (FEM), the transition elements between the enriched and standard elements, which are generally referred as the blending, or partially enriched elements, are often crucial for a good performance of the local partition of unity enrichments. In these elements, the enrichment function cannot be reproduced exactly due to the lack of a partition of unity, and blending elements produce unwanted terms into the approximation that cannot be compensated by the standard finite element part of the approximation. In this paper, some optimal X-FEM-type methods reported in literature are employed to study the performance of blending elements in large plastic deformation problems with weak discontinuities. Several numerical examples are solved using the standard X-FEM, the X-FEM with modified enrichment function, the hierarchical X-FEM and the corrected X-FEM technique, and the results are compared with an alternative intrinsic enrichment strategy in large deformation problems.

ARTICLE HISTORY

Received 2 March 2015
Accepted 9 August 2015

KEYWORDS

X-FEM model; large deformations; blending elements; weak discontinuities

1. Introduction

It is well established that the conventional finite element method (FEM) lacks the accuracy and convergence rate when the exact solution of differential equation or its gradients have singularities or discontinuities. These issues are common in fracture mechanics, contact problems, bimaterial structures, two-phase flow, etc. In such cases, a considerable mesh refinement or the use of higher order elements is required which result in high computational cost and numerical difficulties. Hence, special care must be taken for approximating non-smooth solutions with the FEM. The extended finite element method (X-FEM) offers the inclusion of a priori known solution properties into the approximation space. The simulation is generally carried out on a fixed, simple, structured mesh so that the mesh

construction and continuation are reduced to a minimum. In the X-FEM, the approximation field is enhanced by adding the enrichment functions in the framework of the partition of unity FEM, and is expected to improve the approximation quality and the convergence rate (Belytschko & Black, 1999). However, it was observed that although the accuracy of solution increases with higher order elements, the convergence rate becomes worse in the standard X-FEM; Stazi, Budyn, Chessa, and Belytschko (2003) employed the higher order elements to model the curved crack problem, and observed that the optimal convergence rate cannot be achieved with the X-FEM. It was approved by researchers that the *blending* elements in the transitional zone between the fully enriched and the standard elements are responsible for the lack of optimal convergence rate. In these elements, the partition of unity is violated and the parasitic terms produce the error into the solution space, which result in the poorly conditioned stiffness matrices, the high condition numbers and an increase in the effort required solving the system of equations numerically.

Basically, there are two important issues with the blending elements in the X-FEM; firstly, the enrichment function can no longer be reproduced exactly due to the lack of a partition of unity, and secondly blending elements produce unwanted terms into the approximation which cannot be compensated by the standard finite element (FE) part of the approximation. Thus, a special treatment is required in blending elements to remove the unwanted terms. There are various techniques proposed in literature to overcome those issues related to the parasitic terms in the X-FEM blending elements. Chessa, Wang, and Belytschko (2003) employed the enhanced strain method, or *p*-refinement, in the blending elements to improve the performance of local partition of unity enrichments. The enhanced strain elements were used only in the blending subdomains for any arbitrary enrichment functions, but for each enrichment function a set of enhanced strains must be constructed. Laborde, Pommier, Renard, and Salaün (2005) modified the standard X-FEM to circumvent problems in blending elements for the case of crack problems by enriching a whole fixed area around the crack-tip. It was shown that the 'fixed enrichment area' around the crack-tip can be used efficiently to achieve the expected optimal rate of convergence. Fries and Belytschko (2006) developed an intrinsic X-FEM without blending elements for treating arbitrary discontinuities in a FE context, where no additional unknowns were introduced at the nodes whose supports are crossed by discontinuities. A corrected X-FEM was introduced by Fries (2008), which has two important differences with the standard X-FEM; firstly, in addition to those nodes that are enriched in the standard X-FEM, all nodal points in the blending elements are enriched. Secondly, the enrichment functions of the standard X-FEM are modified except in the reproducing elements, in which they are zero in the standard elements, and they vary continuously between the standard and reproducing elements in the blending elements. In the corrected X-FEM, the modified enrichment function can be reproduced exactly everywhere in the

domain, and the original enrichment function in the reproducing elements. An alternative technique was developed by Gracie, Wang, and Belytschko (2008) based on a discontinuous Galerkin (DG) X-FEM approach to circumvent the spurious behaviour of the blending elements. In the DG-XFEM, the domain is decomposed into non-overlapping patches; in which the enrichments are applied over these patches, and continuity between the patches is enforced using an internal penalty method. Ventura, Gracie, and Belytschko (2009) introduced a weight function blending, where the enrichment function was pre-multiplied by a smooth weight function with a compact support to allow for a completely smooth transition between the enriched and unenriched subdomains. Tarancón, Vercher, Giner, and Fuenmayor (2009) employed the higher order hierarchical shape functions to reduce unwanted effects of the partial enrichment in the blending elements. Shibamura and Utsunomiya (2009) presented an alternative formulation for the X-FEM based on the concept of the partition of unity FEM for solving the problem of blending elements, which assures the numerical accuracy in the entire domain. Loehnert, Mueller-Hoeppe, and Wriggers (2011) extended the originally corrected X-FEM presented by Fries to 3D case with its extension to finite deformation theory. Gupta, Duarte, Babuška, and Banerjee (2015) developed an enrichment scheme based on singular bases and linear polynomials to obtain an optimal convergence of the stable generalised FEM for 3D fractures that lead to the same rate of growth in condition number as the standard FEM for proper choice of singular enrichment functions.

In order to achieve the higher accuracy and convergence rates than the standard FEM, especially in the presence of incompressibility, singularities or distorted meshes, a stabilised conforming nodal integration FEM based on the strain smoothing stabilisation technique was presented by Nguyen-Xuan, Bordas, and Nguyen-Dang (2007). The strain smoothing technique was employed within the partition of unity framework by Natarajan et al. (2008) and Bordas et al. (2010), namely the smoothed X-FEM, to compute and integrate the derivatives of shape functions, which are singular at the crack tip in linear elastic fracture mechanics. A strain smoothing procedure was applied by Chen et al. (2012) on the basis of an edge-based smoothed X-FEM in linear elastic fracture mechanics to outperform the standard X-FEM. In the present paper, some optimal X-FEM-type methods including the extrinsic and intrinsic enrichment strategies are employed to study the performance of blending elements in large plastic deformation problems with weak discontinuities. A computational framework based on the Hu–Washizu assumed strain method is developed for X-FEM large deformations that can be compared with the strain smoothing stabilisation technique proposed in the literature. Several numerical examples are solved using the standard X-FEM, the X-FEM with modified enrichment function, the hierarchical X-FEM and the corrected X-FEM technique, and the results are compared with an alternative intrinsic enrichment strategy proposed here in large deformation problems.

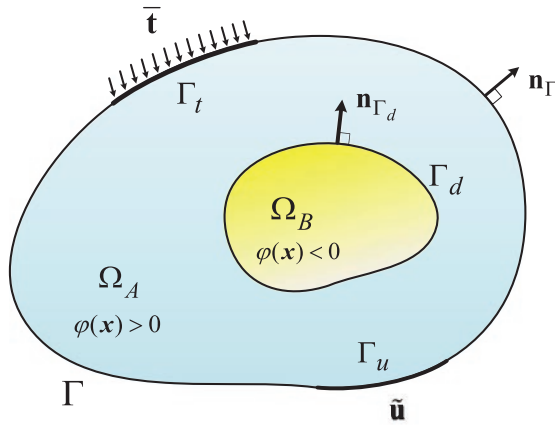


Figure 1. Problem definition of a domain with the weak discontinuity; A schematic view of the bimaterial interface where the displacement is continuous across the interface and the derivatives (strains) are discontinuous.

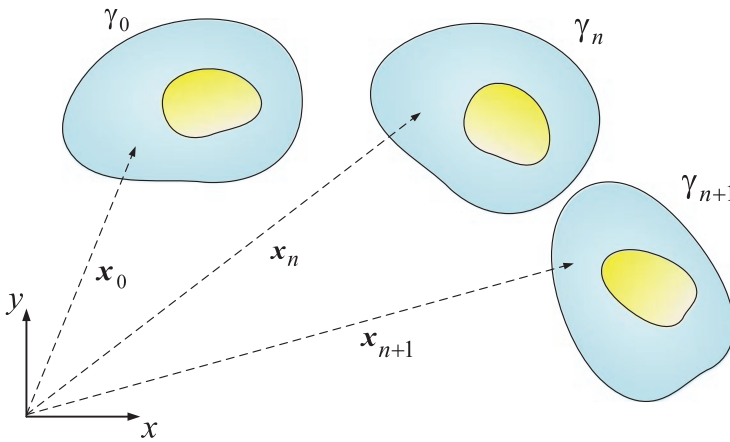


Figure 2. The Lagrangian framework; the initial configuration γ_0 , the known current configuration γ_n and the unknown incremental configuration γ_{n+1} .

2. Large FE deformation formulation

In non-linear problems, non-linearities arise from three distinct sources; constitutive non-linearity, geometric non-linearity and non-linearity in boundary conditions; these are due to material behaviour, large deformations and contact constraints problem, respectively. Consider a body Ω with the boundary Γ subjected to the body force loading \mathbf{b} in Ω , the prescribed traction \mathbf{t} and displacement $\tilde{\mathbf{u}}$ on Γ_t and Γ_u , respectively, and the traction \mathbf{t}_d on the discontinuity surface Γ_d , as shown in Figure 1. It is assumed that the state variables are known at step n , and it is aimed to obtain the variables at step $n + 1$, as shown in Figure 2. Since the configuration of step $n + 1$ is not known, the first Piola–Kirchhof (PK1) stress is generally used to define the equilibrium equation on the available configuration

of step n . This is the core idea of an updated Lagrangian framework; hence, the governing equation of the system can be written as:

$$\nabla_n \cdot \mathbf{P} + \mathbf{b} = 0 \quad (1)$$

where ∇_n is the gradient operator with respect to \mathbf{x}_n , and \mathbf{P} is the first Piola–Kirchhof stress tensor. The boundary conditions are as follows; $\mathbf{u} = \tilde{\mathbf{u}}$ on Γ_u , $\boldsymbol{\sigma} \cdot \mathbf{n} = \mathbf{t}$ on Γ_p , and $\boldsymbol{\sigma} \cdot \mathbf{n} = \mathbf{t}_d$ on Γ_d , with $\boldsymbol{\sigma}$ denoting the Cauchy stress tensor defined on the current configuration.

The weak form of above equation can be obtained by multiplying the test function $\delta \mathbf{u}$ and integrating over the domain as:

$$\int_{\Omega} \delta \mathbf{u} \cdot (\nabla_n \cdot \mathbf{P} + \mathbf{b}) \, d\Omega = 0 \quad (2)$$

Applying the Gauss–Green theorem, it yields to:

$$\int_{\Omega} \nabla_n \delta \mathbf{u} : \mathbf{P} \, d\Omega = \int_{\Gamma_t} \delta \mathbf{u} \cdot \bar{\mathbf{t}} \, d\Gamma + \int_{\Omega} \delta \mathbf{u} \cdot \mathbf{b} \, d\Omega \quad (3)$$

where $\bar{\mathbf{t}}$ is the traction relating to the PK1 stress, Since $\mathbf{x}_{n+1} = \mathbf{x}_n + \mathbf{u}$ with \mathbf{x}_n denoting the vector of coordinates in the current configuration at step n , the deformation gradient can be defined by $\mathbf{F}_n = \mathbf{I} + \partial \mathbf{u} / \partial \mathbf{x}_n$, and the variation of deformation gradient can be given by $\delta \mathbf{F}_n = \partial \delta \mathbf{u} / \partial \mathbf{x}_n$. Substituting the above expressions into Equation (3) yields to:

$$\int_{\Omega} \delta \mathbf{F}_n^T \mathbf{P} \, d\Omega = \int_{\Gamma_t} \delta \mathbf{u}^T \bar{\mathbf{t}} \, d\Gamma + \int_{\Omega} \delta \mathbf{u}^T \mathbf{b} \, d\Omega \quad (4)$$

Since there is of little interest to express the nodal forces in terms of the non-symmetric PK1 stress tensor \mathbf{P} , the second Piola–Kirchhof stress \mathbf{S} can therefore be employed using $\mathbf{P} = \mathbf{F}_n \mathbf{S}$, hence:

$$\int_{\Omega} \delta \mathbf{F}_n^T \mathbf{F}_n \mathbf{S} \, d\Omega = \int_{\Gamma_t} \delta \mathbf{u}^T \bar{\mathbf{t}} \, d\Gamma + \int_{\Omega} \delta \mathbf{u}^T \mathbf{b} \, d\Omega \quad (5)$$

in which the second PK stress is work conjugate stress to the Green strain \mathbf{E}^G defined by $\mathbf{E}^G = \frac{1}{2}(\mathbf{F}_n^T \mathbf{F}_n - \mathbf{I})$; and the variational form of \mathbf{E}^G can be given as $\delta \mathbf{E}^G = \frac{1}{2}(\delta \mathbf{F}_n^T \mathbf{F}_n + \mathbf{F}_n^T \delta \mathbf{F}_n)$. Substituting the aforementioned relations into Equation (5) results in:

$$\int_{\Omega} \delta \mathbf{E}^G \mathbf{S} \, d\Omega = \int_{\Gamma_t} \delta \mathbf{u}^T \bar{\mathbf{t}} \, d\Gamma + \int_{\Omega} \delta \mathbf{u}^T \mathbf{b} \, d\Omega \quad (6)$$

Applying the FE Galerkin discretization, the independent approximations of \mathbf{u} can be defined as $\mathbf{u} = \mathbf{N}\bar{\mathbf{u}}$, with \mathbf{N} denoting the matrix of shape functions and $\bar{\mathbf{u}}$ is the vector of corresponding nodal DOFs. Based on the Green strain tensor, the strain–displacement relationship can be defined in terms of the linear and non-linear components as $\mathbf{E}^G = \mathbf{E}_L + \mathbf{E}_{NL}$, where $\mathbf{E}_L = \mathbf{B}_L\bar{\mathbf{u}}$ and $\mathbf{E}_{NL} = \frac{1}{2}\mathbf{A}_\theta\mathbf{G}\bar{\mathbf{u}}$, in which \mathbf{A}_θ is a function of $\bar{\mathbf{u}}$ defined as:

$$\mathbf{A}_\theta = \begin{bmatrix} \frac{\partial u}{\partial x_n} & \frac{\partial v}{\partial x_n} & 0 & 0 \\ 0 & 0 & \frac{\partial u}{\partial y_n} & \frac{\partial v}{\partial y_n} \\ \frac{\partial u}{\partial y_n} & \frac{\partial v}{\partial y_n} & \frac{\partial u}{\partial x_n} & \frac{\partial v}{\partial x_n} \end{bmatrix} \quad (7)$$

and \mathbf{B}_L is the standard matrix of shape function gradients and \mathbf{G} is the matrix of shape function derivatives defined for node I as:

$$(\mathbf{B}_L)_I = \begin{bmatrix} \frac{\partial N_I}{\partial x_n} & 0 \\ 0 & \frac{\partial N_I}{\partial y_n} \\ \frac{\partial N_I}{\partial y_n} & \frac{\partial N_I}{\partial x_n} \end{bmatrix}, \mathbf{G}_I = \begin{bmatrix} \frac{\partial N_I}{\partial x_n} & 0 \\ 0 & \frac{\partial N_I}{\partial x_n} \\ \frac{\partial N_I}{\partial y_n} & 0 \\ 0 & \frac{\partial N_I}{\partial y_n} \end{bmatrix} \quad (8)$$

Consider $\mathbf{B}_{NL} = \mathbf{A}_\theta\mathbf{G}$, it can be deduced that $d\mathbf{E}^G = (\mathbf{B}_L + \mathbf{B}_{NL}) d\bar{\mathbf{u}}$. Thus, the FE formulation (6) can be obtained as:

$$\boldsymbol{\psi}(\bar{\mathbf{u}}) \equiv \mathbf{F}_{\text{int}} - \mathbf{F}_{\text{ext}} = \int_{\Omega} \bar{\mathbf{B}}^T \mathbf{S} d\Omega - \int_{\Gamma_t} \mathbf{N}^T \bar{\mathbf{t}} d\Gamma - \int_{\Omega} \mathbf{N}^T \mathbf{b} d\Omega = 0 \quad (9)$$

where $\boldsymbol{\psi}$ is the residual vector and $\bar{\mathbf{B}} = \mathbf{B}_L + \mathbf{B}_{NL}$. The above non-linear system of equations must be solved for $\bar{\mathbf{u}}$. The Newton–Raphson method can be used to linearise Equation (9) as:

$$\boldsymbol{\psi}_{n+1}^{i+1}(\bar{\mathbf{u}}) \simeq \boldsymbol{\psi}_{n+1}^i(\bar{\mathbf{u}}) + \left(\frac{\partial \boldsymbol{\psi}}{\partial \bar{\mathbf{u}}} \right)_{n+1}^i d\bar{\mathbf{u}}_n^i = 0 \quad (10)$$

where i refers to i th iteration of the Newton–Raphson method, and $n + 1$ refers to step $n + 1$. In Equation (10), $\partial\boldsymbol{\psi}/\partial\bar{\mathbf{u}}$ can be obtained by taking derivation from (9) as (Khoei, 2005):

$$\begin{aligned} d\boldsymbol{\psi}(\bar{\mathbf{u}}) &= \int_{\Omega} d\bar{\mathbf{B}}^T \mathbf{S} d\Omega + \int_{\Omega} \bar{\mathbf{B}}^T d\mathbf{S} d\Omega \\ &= \left(\int_{\Omega} \mathbf{G}^T \mathbf{M}_S \mathbf{G} d\Omega + \int_{\Omega} \bar{\mathbf{B}}^T \mathbf{C}^{ep} \bar{\mathbf{B}} d\Omega \right) d\bar{\mathbf{u}} \equiv \mathbf{K}_T d\bar{\mathbf{u}} \end{aligned} \quad (11)$$

in which the first integral denotes the geometric stiffness and the second integral indicates the material stiffness. In the above equation, the hypoelasto-plastic

constitutive relation is employed as $d\mathbf{S} = \mathbf{C}^{ep} d\mathbf{E}^G$, in which the tensor \mathbf{C}^{ep} can be obtained from the constitutive law definition with respect to the incremental PK2 stress. The matrix \mathbf{M}_S in (11) is defined as:

$$\mathbf{M}_S = \begin{bmatrix} S_{xx} \mathbf{I}_{2 \times 2} & S_{xy} \mathbf{I}_{2 \times 2} \\ \text{sym.} & S_{yy} \mathbf{I}_{2 \times 2} \end{bmatrix} \quad (12)$$

where \mathbf{I} is the identity matrix. Substituting (11) into (10), the incremental nodal displacements can be obtained in an iterative procedure through the following equation as:

$$(\mathbf{K}_T)_{n+1}^i d\bar{\mathbf{u}}_n^i = -\boldsymbol{\psi}_{n+1}^i \quad (13)$$

In order to solve the system of equations, the residual vector $\boldsymbol{\psi}_{n+1}^i$ is set to load increment $\Delta \mathbf{F}_{\text{ext}}$ at the first iteration of step $n + 1$. The incremental nodal displacements $d\bar{\mathbf{u}}$ can be obtained using the updated values of stresses and strains obtained from the constitutive relation. For the next iteration, the residual vector $\boldsymbol{\psi}_{n+1}^i$ is obtained from (9) and the incremental displacement vector $d\bar{\mathbf{u}}$ from (10). This iterative procedure continues until the norm of residual vector becomes less than the prescribed tolerance. It must be noted that the stiffness matrix \mathbf{K}_T must be updated at each iteration of the Newton–Raphson method. If the convergence of solution is obtained, the nodal coordinates are updated and the PK2 stresses are transferred to the Cauchy stresses at the new configuration by $\boldsymbol{\sigma} = J^{-1} \mathbf{F}_n \mathbf{S} \mathbf{F}_n^T$, where J is the determinant of \mathbf{F}_n .

3. Large X-FEM deformation discretization

In the X-FEM, the discontinuities are taken into account by adding appropriate functions into the standard approximation space through a partition of unity method (PUM), where the singularities and high gradients can be achieved by an optimal convergence rate. The PUM allows the inclusion of prior knowledge of the problem to the FEM space and provides the ability to construct the FEM space of any desired regularity. It is well known that the FEM shape functions $N_I(\mathbf{x})$ constitute the partition of unity. For an enriched element with the shape functions $N_I(\mathbf{x})$ and the enrichment function $\boldsymbol{\psi}(\mathbf{x})$, the displacement field $\mathbf{u}^h(\mathbf{x})$ can be defined as:

$$\mathbf{u}^h(\mathbf{x}) = \mathbf{u}^{\text{std}}(\mathbf{x}) + \mathbf{u}^{\text{enr}}(\mathbf{x}) = \sum_{I \in \mathcal{N}^{\text{std}}} N_I(\mathbf{x}) \bar{\mathbf{u}}_I + \sum_{I \in \mathcal{N}^{\text{enr}}} N_I(\mathbf{x}) \boldsymbol{\psi}(\mathbf{x}) \bar{\mathbf{a}}_I \quad (14)$$

where \mathcal{N}^{std} and \mathcal{N}^{enr} are the set of standard and enriched nodal points, respectively, where $\mathcal{N} = \mathcal{N}^{\text{std}} \cup \mathcal{N}^{\text{enr}}$ is the set of all nodal points. In the above relation, $\bar{\mathbf{u}}_I$ and $\bar{\mathbf{a}}_I$ are the relevant nodal degrees of freedom and \mathbf{x} is the position vector.

The enrichment function $\psi(\mathbf{x})$ is taken as the distance function, the frequently used enrichment function for weak discontinuities, defined as the absolute value of the signed distance function, i.e. $\psi(\mathbf{x}) = |\varphi(\mathbf{x})|$ (Figure 1). The standard level set function, or the signed distance function can be defined as:

$$\varphi(\mathbf{x}) = \|\mathbf{x} - \mathbf{x}_{\Gamma_d}\| \operatorname{sign}\left(\left(\mathbf{x} - \mathbf{x}_{\Gamma_d}\right) \cdot \mathbf{n}_{\Gamma_d}\right) \quad (15)$$

where \mathbf{x}_{Γ_d} is the closest point projection of \mathbf{x} onto the material interface, and $\|\cdot\|$ denotes the Euclidean norm; accordingly, $\|\mathbf{x} - \mathbf{x}_{\Gamma_d}\|$ specifies the distance of point \mathbf{x} to the material interface. Through this definition, the interface can be represented implicitly as the zero iso-contour of the level set function. The signed distance function is continuous, whereas its gradient is discontinuous across Γ_d . Based on this desirable property, the chosen enrichment function enables the approximate displacement field to be discontinuous in its derivatives across Γ_d . Thus, the strain field discontinuity across the material interface can be obtained. However, using the signed distance function in the standard X-FEM approximation (14) may significantly degrade both the accuracy and the overall convergence rate of the solution. The reason for the decrease in the accuracy and the suboptimal convergence rate is that this choice of enrichment leads to problems in the blending elements, as discussed in the next section.

In practice a shifted version of relation (14) is generally used, in which the nodal displacements take the actual value of $\bar{\mathbf{u}}_I$ and the effect of enrichment is alleviated. This formulation has several advantages; for instance, the Dirichlet boundary conditions can be applied without any modification compared to the standard FEM. The shifted X-FEM displacement field can be defined as:

$$\mathbf{u}^h(\mathbf{x}) = \sum_{I \in \mathcal{N}^{\text{std}}} N_I(\mathbf{x}) \bar{\mathbf{u}}_I + \sum_{I \in \mathcal{N}^{\text{enr}}} N_I(\mathbf{x}) (\psi(\mathbf{x}) - \psi(\mathbf{x}_I)) \bar{\mathbf{a}}_I \quad (16)$$

In order to model the weak discontinuities in large deformations, the Lagrangian formulation is employed in the framework of X-FEM technique (Broumand & Khoei, 2013; Khoei, Biabanaki, & Anahid, 2008, 2009). Since the enrichment function $\psi(\mathbf{x})$ is defined on an initial undeformed configuration, an appropriate mapping is used to transfer the values of enrichment functions on the current configuration in an updated Lagrangian framework. In the X-FEM formulation, the current position vector is defined by $\mathbf{x} = \mathbf{x}_0 + \mathbf{u}$, where \mathbf{u} is the total displacement vector and \mathbf{x}_0 is the initial position vector. Based on the X-FEM displacement field (16), the current position vector can be obtained as:

$$\mathbf{x} = \sum_{I \in \mathcal{N}^{\text{std}}} N_I(\xi, \eta) \mathbf{x}_I + \sum_{I \in \mathcal{N}^{\text{enr}}} N_I(\xi, \eta) (\psi(\mathbf{x}) - \psi(\mathbf{x}_I)) \bar{\mathbf{a}}_I \quad (17)$$

where (ξ, η) are defined on the parent element. The Jacobian matrix for the current configuration can be defined as:

$$J = \begin{bmatrix} \frac{\partial x}{\partial \xi} & \frac{\partial y}{\partial \xi} \\ \frac{\partial x}{\partial \eta} & \frac{\partial y}{\partial \eta} \end{bmatrix} \quad (18)$$

in which the components of matrix J are given as:

$$\begin{aligned} J_{11} &= \frac{\partial x}{\partial \xi} = \sum_{I \in \mathcal{N}^{\text{std}}} \frac{\partial N_I}{\partial \xi} x_I + \sum_{I \in \mathcal{N}^{\text{enr}}} \frac{\partial N_I}{\partial \xi} (\psi(\mathbf{x}) - \psi(\mathbf{x}_I)) \bar{\mathbf{a}}_I^x \\ J_{12} &= \frac{\partial y}{\partial \xi} = \sum_{I \in \mathcal{N}^{\text{std}}} \frac{\partial N_I}{\partial \xi} y_I + \sum_{I \in \mathcal{N}^{\text{enr}}} \frac{\partial N_I}{\partial \xi} (\psi(\mathbf{x}) - \psi(\mathbf{x}_I)) \bar{\mathbf{a}}_I^y \\ J_{21} &= \frac{\partial x}{\partial \eta} = \sum_{I \in \mathcal{N}^{\text{std}}} \frac{\partial N_I}{\partial \eta} x_I + \sum_{I \in \mathcal{N}^{\text{enr}}} \frac{\partial N_I}{\partial \eta} (\psi(\mathbf{x}) - \psi(\mathbf{x}_I)) \bar{\mathbf{a}}_I^x \\ J_{22} &= \frac{\partial y}{\partial \eta} = \sum_{I \in \mathcal{N}^{\text{std}}} \frac{\partial N_I}{\partial \eta} y_I + \sum_{I \in \mathcal{N}^{\text{enr}}} \frac{\partial N_I}{\partial \eta} (\psi(\mathbf{x}) - \psi(\mathbf{x}_I)) \bar{\mathbf{a}}_I^y \end{aligned} \quad (19)$$

In the same manner, the matrices \mathbf{B}_L , \mathbf{B}_{NL} and \mathbf{G} given in Equation (11) can be defined for the X-FEM formulation using the enrichment displacement field. Applying the enrichment displacement field (16) into these matrices results in two distinct parts, including the standard and enriched parts defined for node I as:

$$(\mathbf{B}_L^{\text{std}})_I = \begin{bmatrix} \frac{\partial N_I}{\partial x_n} & 0 \\ 0 & \frac{\partial N_I}{\partial y_n} \\ \frac{\partial N_I}{\partial y_n} & \frac{\partial N_I}{\partial x_n} \end{bmatrix}, \quad (\mathbf{B}_L^{\text{enr}})_I = \begin{bmatrix} \frac{\partial}{\partial x_n} (N_I(\mathbf{x})\bar{\psi}(\mathbf{x})) & 0 \\ 0 & \frac{\partial}{\partial y_n} (N_I(\mathbf{x})\bar{\psi}(\mathbf{x})) \\ \frac{\partial}{\partial y_n} (N_I(\mathbf{x})\bar{\psi}(\mathbf{x})) & \frac{\partial}{\partial x_n} (N_I(\mathbf{x})\bar{\psi}(\mathbf{x})) \end{bmatrix} \quad (20)$$

Similarly, the standard and enriched parts of the non-linear matrix \mathbf{B}_{NL} can be obtained using $\mathbf{B}_{NL} = \mathbf{A}_\theta \mathbf{G}$ as:

$$(\mathbf{B}_{NL}^{\text{std}})_I = \begin{bmatrix} \frac{\partial u}{\partial x_n} \frac{\partial N_I}{\partial x_n} & \frac{\partial v}{\partial x_n} \frac{\partial N_I}{\partial x_n} \\ \frac{\partial u}{\partial y_n} \frac{\partial N_I}{\partial y_n} & \frac{\partial v}{\partial y_n} \frac{\partial N_I}{\partial y_n} \\ \frac{\partial u}{\partial x_n} \frac{\partial N_I}{\partial y_n} + \frac{\partial u}{\partial y_n} \frac{\partial N_I}{\partial x_n} & \frac{\partial v}{\partial x_n} \frac{\partial N_I}{\partial y_n} + \frac{\partial v}{\partial y_n} \frac{\partial N_I}{\partial x_n} \end{bmatrix}, \quad (21)$$

$$(\mathbf{B}_{NL}^{\text{enr}})_I = \begin{bmatrix} \frac{\partial u}{\partial x_n} \frac{\partial}{\partial x_n} (N_I(\mathbf{x})\bar{\psi}(\mathbf{x})) & \frac{\partial v}{\partial x_n} \frac{\partial}{\partial x_n} (N_I(\mathbf{x})\bar{\psi}(\mathbf{x})) \\ \frac{\partial u}{\partial y_n} \frac{\partial}{\partial y_n} (N_I(\mathbf{x})\bar{\psi}(\mathbf{x})) & \frac{\partial v}{\partial y_n} \frac{\partial}{\partial y_n} (N_I(\mathbf{x})\bar{\psi}(\mathbf{x})) \\ \frac{\partial u}{\partial x_n} \frac{\partial}{\partial y_n} (N_I(\mathbf{x})\bar{\psi}(\mathbf{x})) + \frac{\partial u}{\partial y_n} \frac{\partial}{\partial x_n} (N_I(\mathbf{x})\bar{\psi}(\mathbf{x})) & \frac{\partial v}{\partial x_n} \frac{\partial}{\partial y_n} (N_I(\mathbf{x})\bar{\psi}(\mathbf{x})) + \frac{\partial v}{\partial y_n} \frac{\partial}{\partial x_n} (N_I(\mathbf{x})\bar{\psi}(\mathbf{x})) \end{bmatrix}$$

and the standard and enriched parts of matrix \mathbf{G} are defined as:

$$\mathbf{G}_I^{\text{std}} = \begin{bmatrix} \frac{\partial N_I}{\partial x_n} & 0 \\ 0 & \frac{\partial N_I}{\partial x_n} \\ \frac{\partial N_I}{\partial y_n} & 0 \\ 0 & \frac{\partial N_I}{\partial y_n} \end{bmatrix}, \quad \mathbf{G}_I^{\text{enr}} = \begin{bmatrix} \frac{\partial}{\partial x_n} (N_I(\mathbf{x})\bar{\psi}(\mathbf{x})) & 0 \\ 0 & \frac{\partial}{\partial x_n} (N_I(\mathbf{x})\bar{\psi}(\mathbf{x})) \\ \frac{\partial}{\partial y_n} (N_I(\mathbf{x})\bar{\psi}(\mathbf{x})) & 0 \\ 0 & \frac{\partial}{\partial y_n} (N_I(\mathbf{x})\bar{\psi}(\mathbf{x})) \end{bmatrix} \quad (22)$$

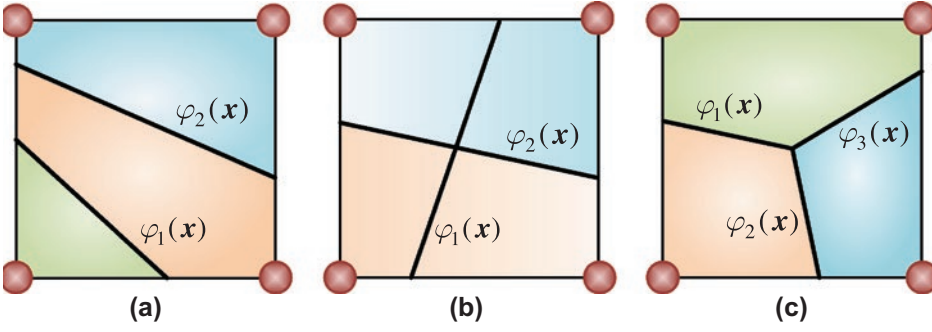


Figure 3. Multiple material interfaces; (a) an element cut by two separated interfaces $\varphi_1(\mathbf{x})$ and $\varphi_2(\mathbf{x})$, (b) two interfaces $\varphi_1(\mathbf{x})$ and $\varphi_2(\mathbf{x})$ intersect in an element and (c) multiple interfaces intersect in an element.

where $\bar{\psi}(\mathbf{x}) = (\psi(\mathbf{x}) - \psi(\mathbf{x}_I))$. Finally, the non-linear system of Equation (13) for large X-FEM deformation problems can be obtained as:

$$\begin{bmatrix} \mathbf{K}_T^{\text{std}, \text{std}} & \mathbf{K}_T^{\text{std}, \text{enr}} \\ \mathbf{K}_T^{\text{enr}, \text{std}} & \mathbf{K}_T^{\text{enr}, \text{enr}} \end{bmatrix}_{n+1}^i \begin{Bmatrix} d\bar{\mathbf{u}} \\ d\bar{\mathbf{a}} \end{Bmatrix}_n^i = - \begin{Bmatrix} \boldsymbol{\psi}^{\text{std}} \\ \boldsymbol{\psi}^{\text{enr}} \end{Bmatrix}_{n+1}^i \quad (23)$$

where $\boldsymbol{\psi}^{\text{std}} = \mathbf{F}_{\text{int}}^{\text{std}} - \mathbf{F}_{\text{ext}}^{\text{std}}$ and $\boldsymbol{\psi}^{\text{enr}} = \mathbf{F}_{\text{int}}^{\text{enr}} - \mathbf{F}_{\text{ext}}^{\text{enr}}$. In the above system of equations, the components of the total stiffness matrix and the external force vector are defined as:

$$\mathbf{K}_T^{\alpha\beta} = \int_{\Omega} \mathbf{G}^{\alpha T} \mathbf{M}_S \mathbf{G}^{\beta} d\Omega + \int_{\Omega} \bar{\mathbf{B}}^{\alpha T} \mathbf{C}^{ep} \bar{\mathbf{B}}^{\beta} d\Omega \quad (24\text{-a})$$

$$\mathbf{F}_{\text{ext}}^{\alpha} = \int_{\Gamma_I} \mathbf{N}^{\alpha T} \bar{\mathbf{t}} d\Gamma + \int_{\Omega} \mathbf{N}^{\alpha T} \mathbf{b} d\Omega \quad (24\text{-b})$$

where $(\alpha, \beta) \in (\text{std}, \text{enr})$; and $\mathbf{N}^{\text{std}} = \mathbf{N}(\mathbf{x})$ and $\mathbf{N}^{\text{enr}} = \mathbf{N}(\mathbf{x})(\psi(\mathbf{x}) - \psi(\mathbf{x}_I))$.

3.1. Multiple interfaces

In the X-FEM formulation described above, the displacement approximation $\mathbf{u}^h(\mathbf{x})$ is defined for only one unique interface. In the case that an element intersects with multiple interfaces the enriched part of Equation (14) must include additional enrichment functions. Consider the case that the interfaces intersecting with an element are assumed to be geometrically separated from each other where there exist no intersections between the interfaces, the X-FEM approximation field (14) for modelling of multiple material interfaces can be written as:

$$\mathbf{u}^h(\mathbf{x}) = \sum_{I \in \mathcal{N}^{\text{std}}} N_I(\mathbf{x}) \bar{\mathbf{u}}_I + \sum_{\mathcal{K}} \sum_{I \in \mathcal{N}^{\text{enr}}} N_I(\mathbf{x}) \psi_{\mathcal{K}}(\mathbf{x}) \bar{\mathbf{a}}_I^{\mathcal{K}} \quad (25)$$

where the enrichment function $\psi_{\mathcal{K}}$ is the absolute value of the signed distance function $\varphi_{\mathcal{K}}(\mathbf{x})$, i.e. $\psi_{\mathcal{K}}(\mathbf{x}) = |\varphi_{\mathcal{K}}(\mathbf{x})|$, and $\bar{\mathbf{a}}_I^{\mathcal{K}}$ is the relevant enriched nodal degrees of freedom corresponding to material interface \mathcal{K} . Figure 3(a) illustrates an element cut by two separated material interfaces $\varphi_1(\mathbf{x})$ and $\varphi_2(\mathbf{x})$. The shifted version of X-FEM displacement field (25) can be written as:

$$\mathbf{u}^h(\mathbf{x}) = \sum_{I \in \mathcal{N}^{\text{std}}} N_I(\mathbf{x}) \bar{\mathbf{u}}_I + \sum_{\mathcal{K}} \sum_{I \in \mathcal{N}^{\text{enr}}} N_I(\mathbf{x}) (\psi_{\mathcal{K}}(\mathbf{x}) - \psi_{\mathcal{K}}(\mathbf{x}_I)) \bar{\mathbf{a}}_I^{\mathcal{K}} \quad (26)$$

In the case that an element intersects with multiple material interfaces whose support contains intersecting interfaces, the displacement field (25) must include additional enrichment functions. For example, consider the case that two interfaces $\varphi_1(\mathbf{x})$ and $\varphi_2(\mathbf{x})$ intersect in an element, as shown in Figure 3(b), the X-FEM approximation field can be defined as:

$$\mathbf{u}^h(\mathbf{x}) = \sum_{I \in \mathcal{N}^{\text{std}}} N_I(\mathbf{x}) \bar{\mathbf{u}}_I + \sum_{I \in \mathcal{N}^{\text{enr}}} N_I(\mathbf{x}) \psi_1(\mathbf{x}) \bar{\mathbf{a}}_I + \sum_{I \in \mathcal{N}^{\text{enr}}} N_I(\mathbf{x}) \psi_2(\mathbf{x}) \bar{\mathbf{b}}_I + \sum_{I \in \mathcal{N}^{\text{enr}}} N_I(\mathbf{x}) \psi_1(\mathbf{x}) \psi_2(\mathbf{x}) \bar{\mathbf{c}}_I \quad (27)$$

in which the enrichment functions $\psi_1(\mathbf{x})$ and $\psi_2(\mathbf{x})$ are respectively chosen as the absolute value of the signed distance functions $\varphi_1(\mathbf{x})$ and $\varphi_2(\mathbf{x})$, i.e. $\psi_1(\mathbf{x}) = |\varphi_1(\mathbf{x})|$ and $\psi_2(\mathbf{x}) = |\varphi_2(\mathbf{x})|$. The shifted version of displacement field (27) can be written as:

$$\begin{aligned} \mathbf{u}^h(\mathbf{x}) = & \sum_{I \in \mathcal{N}^{\text{std}}} N_I(\mathbf{x}) \bar{\mathbf{u}}_I + \sum_{I \in \mathcal{N}^{\text{enr}}} N_I(\mathbf{x}) (\psi_1(\mathbf{x}) - \psi_1(\mathbf{x}_I)) \bar{\mathbf{a}}_I + \sum_{I \in \mathcal{N}^{\text{enr}}} N_I(\mathbf{x}) (\psi_2(\mathbf{x}) - \psi_2(\mathbf{x}_I)) \bar{\mathbf{b}}_I \\ & + \sum_{I \in \mathcal{N}^{\text{enr}}} N_I(\mathbf{x}) (\psi_1(\mathbf{x}) \psi_2(\mathbf{x}) - \psi_1(\mathbf{x}_I) \psi_2(\mathbf{x}_I)) \bar{\mathbf{c}}_I \end{aligned} \quad (28)$$

It must be noted that an additional enrichment function proposed in the last term of relations (27) and (28) is called as the *junction ramp* enrichment function. This enrichment function is continuous over the element and has a discontinuous gradient in the direction perpendicular to the line segments. In fact, in the case that multiple interfaces intersect inside an element, as shown in Figure 3(c), the *junction ramp* enrichment function is defined based on multiplication of the distance-level set functions obtained from two line segments Γ_i and Γ_j as:

$$\mathcal{J}(\mathbf{x}) = |\varphi_i(\mathbf{x})| |\varphi_j(\mathbf{x})| \quad (29)$$

Thus, the enriched displacement field (28) can be rewritten for multiple interfaces intersect inside an element as:

$$\mathbf{u}^h(\mathbf{x}) = \sum_{I \in \mathcal{N}^{\text{std}}} N_I(\mathbf{x}) \bar{\mathbf{u}}_I + \sum_{\mathcal{K}} \sum_{I \in \mathcal{N}^{\text{enr}}} N_I(\mathbf{x}) (\psi_{\mathcal{K}}(\mathbf{x}) - \psi_{\mathcal{K}}(\mathbf{x}_I)) \bar{\mathbf{a}}_I^{\mathcal{K}} + \sum_{I \in \mathcal{N}^{\text{enr}}} N_I(\mathbf{x}) (\mathcal{J}(\mathbf{x}) - \mathcal{J}(\mathbf{x}_I)) \bar{\mathbf{d}}_I \quad (30)$$

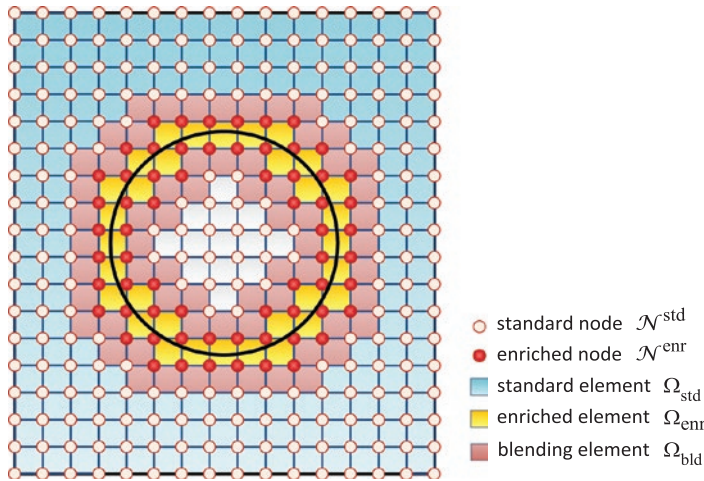


Figure 4. The domain of problem in X-FEM illustrating the enriched subdomain Ω_{enr} , the standard subdomain Ω_{std} and the partially enriched subdomain Ω_{bld} .

4. Blending strategies in X-FEM

In the X-FEM, the problem domain Ω is generally decomposed into three subdomains (Figure 4); the subdomain Ω_{enr} with the set of elements in which their nodal points are fully enriched, the subdomain Ω_{std} that includes the set of elements where their nodal points are not enriched, and the subdomain Ω_{bld} with the set of elements where their nodal points are partially enriched called as the blending elements. Since these elements are ‘partially enriched’, the enriched nodes in these elements do not form a partition of unity. In the X-FEM, there are basically two important issues with the blending elements (Khoei, 2015); the first is related to the partition of unity property of the blending element. In fact, the partition of unity is violated in blending elements since not all nodal points are enriched, i.e. $\sum_{j \in \mathcal{M}^B} N_j(\mathbf{x}) \neq 1$, and consequently the approximation is no longer able to represent the enrichment function $\psi(\mathbf{x})$ exactly, i.e. $\sum_{j \in \mathcal{M}^B} N_j(\mathbf{x})\psi(x_j) \neq \psi(\mathbf{x})$. It means that the enrichment functions cannot be reproduced properly in blending elements. This fact, however, does not pose a severe problem since the capture of local phenomena through the enrichment is more interested.

The next issue that has a significant problem in the X-FEM is the introduction of unwanted terms in the approximation which, in general, cannot be compensated by the standard FE part of the approximation. The appearance of unwanted terms in the blending elements is much more severe than the fact that $\psi(\mathbf{x})$ can no longer be represented exactly. These terms can degrade the convergence of the X-FEM significantly. Thus, a special treatment is necessary in blending elements in order to remove the unwanted terms. There are various methods proposed in literature to alleviate the above problems in blending elements. These approaches that have been developed to improve the accuracy, convergence rate and condition number in the blending elements are the *modified enrichment function* method, the

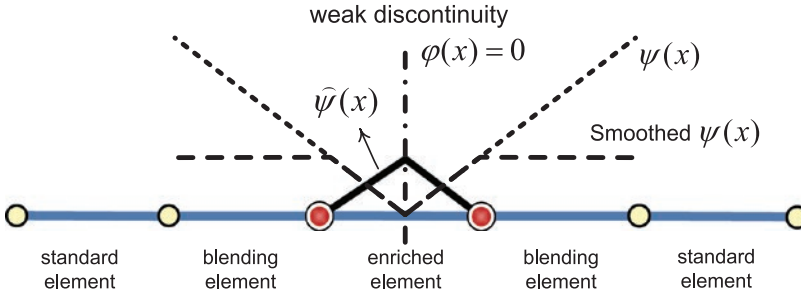


Figure 5. One dimensional representation of various enrichment functions for the material interface problem.

enhanced strain method, the *hierarchical* method, the *cutoff* function method and the *discontinuous Galerkin* (DG) method. In this section, an overview of various techniques proposed to circumvent the errors caused by parasitic terms in the approximation space of the blending elements are presented, and their performances in large plasticity deformation problems will be given in the next section.

4.1. Modified enrichment function method

The modified enrichment function proposed by Moës, Cloirec, Cartraud, and Remacle (2003) is an approach used to improve the accuracy and convergence rate of the standard X-FEM while dealing with the weak discontinuities, such as holes, inclusions and bimaterial problems, where the displacement field is continuous but its derivatives are discontinuous. For such problems, the absolute value of the level set function $\varphi(\mathbf{x})$ can be used as $\psi(\mathbf{x}) = |\varphi(\mathbf{x})|$ which has a discontinuous first derivative on the material interface. It must be noted that the values of level set function are only computed at the nodal points of FE mesh, so the level set function $\varphi(\mathbf{x})$ can be approximated based on the values of nodal points φ_I using the interpolation functions $N_I(\mathbf{x})$ as:

$$\psi(\mathbf{x}) = \left| \sum_I N_I(\mathbf{x}) \varphi_I \right| \quad (31)$$

It was shown by Sukumar, Chopp, Moës, and Belytschko (2001) and Belytschko, Black, Moës, Sukumar, and Usui (2003) that a smoothing function of $\psi(\mathbf{x})$ away from the element layer containing the interface, somewhat improves the accuracy and convergence rate. However, Moës et al. (2003) proposed an alternative definition of the absolute value of level set function $\varphi(\mathbf{x})$ for weak discontinuity problems that shows a better accuracy and convergence rate as:

$$\hat{\psi}(\mathbf{x}) = \sum_{I \in \mathcal{N}^{\text{enr}}} N_I(\mathbf{x}) |\varphi_I| - \left| \sum_{I \in \mathcal{N}^{\text{enr}}} N_I(\mathbf{x}) \varphi_I \right| \quad (32)$$

The main advantage of above enrichment function is that it has a non-zero value only in the elements cut by the interface. The above enrichment function has a ridge centred on the interface and zero value on the elements which are not crossed by the interface, as shown in Figure 5. It must be noted that the enrichment is only required in the subdomain where the local property in the solution is to be captured. In the surrounding subdomain where the conventional smoothness condition is satisfied, the classical FE approximation is capable of approximating the solution closely. In fact, the modified enrichment function (32) is given such that the resulting enrichment function is zero in the blending elements, and the unwanted terms appearing in the approximating space of the blending elements are avoided. This choice of the enrichment function is illustrated to give more accurate numerical results than the standard level set function for a given discretization and to converge optimally.

4.2. Enhanced strain method

An approach to improve the performance of local partition of unity enrichments in the blending elements was introduced by Chessa et al. (2003) based on an enhanced strain method for small deformation problems. According to this method by properly choosing an enhanced strain field, the unwanted terms can be eliminated in the enriched displacement field. The enhanced strain method is a general approach used to overcome the locking issue in incompressible material problems within the framework of a mixed FEM formulation. In this study, the enhanced strain method is used only in the blending domain to eliminate the undesirable terms that arise from the enrichment function in the blending subdomain within the large X-FEM deformation formulation. Based on this method, the assumed strain field $\bar{\mathbf{E}}$ is defined for the large X-FEM deformation based on the sum of the Green strain \mathbf{E}^G and an enhanced strain field \mathbf{E}^{enh} as:

$$\bar{\mathbf{E}} = \mathbf{E}^G + \mathbf{E}^{\text{enh}} \quad (33)$$

in which the enhanced strain \mathbf{E}^{enh} is defined in blending element Ω_{bld} by $\mathbf{E}^{\text{enh}} = \mathbf{N}^{\text{bld}} \bar{\mathbf{b}}$, where \mathbf{N}^{bld} are the shape functions of assumed strain element whose support is limited to Ω_{bld} , and $\bar{\mathbf{b}}$ is the corresponding enhanced vector of DOFs. In the above definition, \mathbf{E}^G is given in terms of the linear and non-linear Green strain tensor by $\mathbf{E}^G = \mathbf{E}_L + \mathbf{E}_{NL}$, where $\delta \mathbf{E}_L = \mathbf{B}_L^{\text{std}} \delta \bar{\mathbf{u}} + \mathbf{B}_L^{\text{enr}} \delta \bar{\mathbf{a}}$ and $\delta \mathbf{E}_{NL} = \mathbf{B}_{NL}^{\text{std}} \delta \bar{\mathbf{u}} + \mathbf{B}_{NL}^{\text{enr}} \delta \bar{\mathbf{a}}$. Applying the variational form of potential energy (6) in the framework of a mixed large X-FEM deformation formulation, it leads to:

$$\int_{\Omega} \delta \bar{\mathbf{E}}^T \mathbf{S}(\bar{\mathbf{E}}) d\Omega = \int_{\Gamma_i} \delta \mathbf{u}^T \bar{\mathbf{t}} d\Gamma + \int_{\Omega} \delta \mathbf{u}^T \mathbf{b} d\Omega \quad (34)$$

It must be noted that in the derivation of above variational formulation, it is assumed that \mathbf{E}^{enh} is orthogonal to the assumed PK2 stress $\bar{\mathbf{S}}$. In Equation (34), $\delta \bar{\mathbf{E}}$

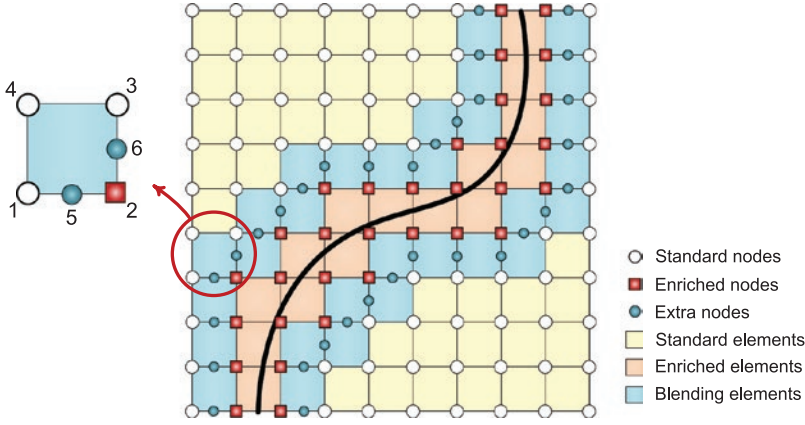


Figure 6. Construction of hierarchical blending elements for the linear four-noded quadrilateral elements.

is defined as $\delta \bar{\mathbf{E}} = \delta \mathbf{E}^G + \delta \mathbf{E}^{\text{enh}}$ where $\delta \mathbf{E}^G = \bar{\mathbf{B}}^{\text{std}} \delta \bar{\mathbf{u}} + \bar{\mathbf{B}}^{\text{enr}} \delta \bar{\mathbf{a}}$ and $\delta \mathbf{E}^{\text{enh}} = \mathbf{N}^{\text{Bld}} \delta \bar{\mathbf{b}}$. Substituting the aforementioned relations into Equation (34) and applying the X-FEM discretization formulation, the non-linear system of Equation (23) for the mixed large X-FEM deformation formulation can be obtained as:

$$\begin{bmatrix}
 \mathbf{K}_T^{\text{std, std}} & \mathbf{K}_T^{\text{std, enr}} & \int_{\Omega} \bar{\mathbf{B}}^{\text{std}^T} \mathbf{C}^{ep} \mathbf{N}^{\text{Bld}} d\Omega \\
 \mathbf{K}_T^{\text{enr, std}} & \mathbf{K}_T^{\text{enr, enr}} & \int_{\Omega} \bar{\mathbf{b}}^{\text{enr}^T} \mathbf{C}^{ep} \mathbf{N}^{\text{Bld}} d\Omega \\
 \int_{\Omega} \mathbf{N}^{\text{Bld}^T} \mathbf{C}^{ep} \bar{\mathbf{B}}^{\text{std}} d\Omega & \int_{\Omega} \mathbf{N}^{\text{Bld}^T} \mathbf{C}^{ep} \bar{\mathbf{B}}^{\text{enr}} d\Omega & \int_{\Omega} \mathbf{N}^{\text{Bld}^T} \mathbf{C}^{ep} \mathbf{N}^{\text{Bld}} d\Omega
 \end{bmatrix}_{n+1}^i \quad (35)$$

$$\begin{Bmatrix} d\bar{\mathbf{u}} \\ d\bar{\mathbf{a}} \\ d\bar{\mathbf{b}} \end{Bmatrix}_n^i = - \begin{Bmatrix} \bar{\boldsymbol{\psi}}^{\text{std}} \\ \bar{\boldsymbol{\psi}}^{\text{enr}} \\ \bar{\boldsymbol{\psi}}^{\text{Bld}} \end{Bmatrix}_{n+1}^i$$

in which the incremental enhanced strain DOFs $d\bar{\mathbf{b}}_n^i$ can be obtained from (35) over each blending element where the shape functions of assumed strain element \mathbf{N}^{Bld} is defined. In order to construct an enhanced strain field \mathbf{E}^{enh} for the blending elements of a problem with the discontinuity in the gradient of displacement where the ramp enrichment function is used, the enhanced strain method described above is utilised by introducing the enhanced strain space \mathcal{S}^{enh} as $\mathcal{S}^{\text{enh}} = \text{span}\{\xi, \eta, \xi\eta, \xi^2 - \eta^2, \xi^2\eta, \xi\eta^2\}$ with respect to the parent coordinates (ξ, η) for a four-noded bilinear element to remove the unwanted terms (Chessa et al., 2003).

4.3. The hierarchical method

An alternative approach to improve the accuracy and convergence rate of local partition of unity enrichments in the blending elements is based on the hierarchical

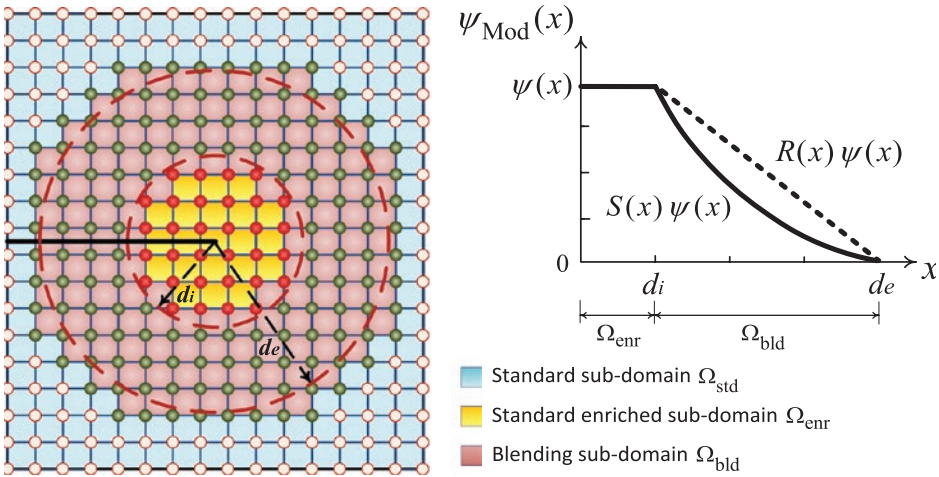


Figure 7. The weight function blending method; decomposition of the enrichment domain into the standard enriched subdomain Ω_{enr} where $S(x) = 1$, and the blending subdomain Ω_{bld} where $0 < S(x) < 1$.

method that utilises different order of polynomials for the standard and enriched shape functions. It was shown by Chessa et al. (2003) that if the order of shape functions of the standard part is higher than the enriched part, the parasitic terms in the blending elements can be corrected by the standard part of the approximation field, and the accuracy and convergence rate of the solution can be improved. They showed that for the polynomial enrichment functions of order p , if the shape function of standard part \mathbf{N}^{std} is s -order complete and the shape function of enriched part \mathbf{N}^{enr} is e -order complete, the parasitic terms can be removed such that $s \geq e + p$. In this case, the displacement field $\mathbf{u}^h(\mathbf{x})$ can reproduce a linear field in the blending elements even if the enrichment is active.

In order to construct the hierarchical shape functions for blending elements in a problem with the discontinuity in the gradient of displacements where the ramp enrichment function $\psi(\mathbf{x}) = |\varphi(\mathbf{x})|$ is used, the standard shape functions of the approximation in Ω_{bld} must be one degree higher than the enriched shape functions. A blending element that satisfies the expression $s \geq e + p$ can be constructed by identifying the fact that pathological terms in the blending elements due to the partial enrichment are quadratic primarily normal to the discontinuity. Thus, it is sufficient to use a hierarchical element with quadratic shape functions on the edges not coincident with the boundary between Ω_{bld} and Ω_{std} . A hierarchical blending element for a linear quadrilateral element can be constructed by adding mid-side nodes to the sides connecting the enriched nodes to the standard nodes of a four-noded element, as shown in Figure 6. The shape functions for the standard and enriched displacement fields $\mathbf{u}^{std}(\mathbf{x})$ and $\mathbf{u}^{enr}(\mathbf{x})$ in the blending elements are defined as:

$$\begin{aligned}
 N_I^{\text{std}}(\xi, \eta) &= \frac{1}{4}(1 + \xi_I \xi)(1 + \eta_I \eta) \quad (I = 1, 2, 3, 4) \\
 N_5^{\text{std}}(\xi, \eta) &= \frac{1}{2}(1 - \xi^2)(1 - \eta) \\
 N_6^{\text{std}}(\xi, \eta) &= \frac{1}{2}(1 + \xi)(1 - \eta^2) \\
 N_2^{\text{enr}}(\xi, \eta) &= \frac{1}{4}(1 + \xi)(1 - \eta)
 \end{aligned} \tag{36}$$

4.4. The cutoff function method

An efficient approach was proposed by Fries (2008) based on a linearly decreasing weight function for the enrichment in the blending elements, called as the modified X-FEM technique. This approach allows to obtain a conforming approximation and to eliminate partially enriched elements, so that the partition of unity property can be satisfied everywhere in the domain. In this method, in addition to those nodes that are enriched in the standard X-FEM, all nodes in the blending elements are enriched that presents a complete partition of unity in the enriched and blending elements. Moreover, the enrichment functions of the standard X-FEM are modified such that they are zero in the standard elements, and vary continuously in the blending elements between the standard and enriched elements. This modification avoids unwanted terms in the blending elements and leads to continuous local enrichment functions as long as the enrichment function $\psi(\mathbf{x})$ is continuous. Based on the corrected X-FEM technique, a modified enrichment function $\psi_{\text{Mod}}(\mathbf{x})$ is defined as:

$$\psi_{\text{Mod}}(\mathbf{x}) = R(\mathbf{x})\psi(\mathbf{x}) \tag{37}$$

where the cutoff function $R(\mathbf{x})$ is defined based on the ramp function as $R(\mathbf{x}) = \sum_{I \in \mathcal{N}^{\text{enr}}} N_I(\mathbf{x})$ with \mathcal{N}^{enr} denotes the set of nodes of those elements located in the enrichment radius. It is obvious that $\psi_{\text{Mod}}(\mathbf{x}) = \psi(\mathbf{x})$ in the enriched elements where their nodes are in \mathcal{N}^{enr} , and $\psi_{\text{Mod}}(\mathbf{x}) = 0$ in the standard FEs. In the blending elements where some nodes are in \mathcal{N}^{enr} , the modified enrichment function $\psi_{\text{Mod}}(\mathbf{x})$ varies continuously between $\psi(\mathbf{x})$ and zero.

By introducing the set of nodes \mathcal{M}^{enr} based on the set of nodes \mathcal{N}^{enr} and all other nodes of the blending elements, a modified version of the enriched approximation field (14) can be written as:

$$\mathbf{u}^h(\mathbf{x}) = \sum_{I \in \mathcal{N}^{\text{std}}} N_I(\mathbf{x}) \bar{\mathbf{u}}_I + \sum_{I \in \mathcal{M}^{\text{enr}}} N_I(\mathbf{x}) \psi_{\text{Mod}}(\mathbf{x}) \bar{\mathbf{a}}_I \tag{38}$$

in which the set of nodes \mathcal{M}^{enr} consists of all element nodes of the enriched and blending elements with $\mathcal{N}^{\text{enr}} \subset \mathcal{M}^{\text{enr}}$. A shifted version of the enriched approximation field (38) can be written as:

$$\mathbf{u}^h(\mathbf{x}) = \sum_{I \in \mathcal{N}^{\text{std}}} N_I(\mathbf{x}) \bar{\mathbf{u}}_I + \sum_{I \in \mathcal{M}^{\text{enr}}} N_I(\mathbf{x}) (\psi_{\text{Mod}}(\mathbf{x}) - \psi_{\text{Mod}}(\mathbf{x}_I)) \bar{\mathbf{a}}_I \tag{39}$$

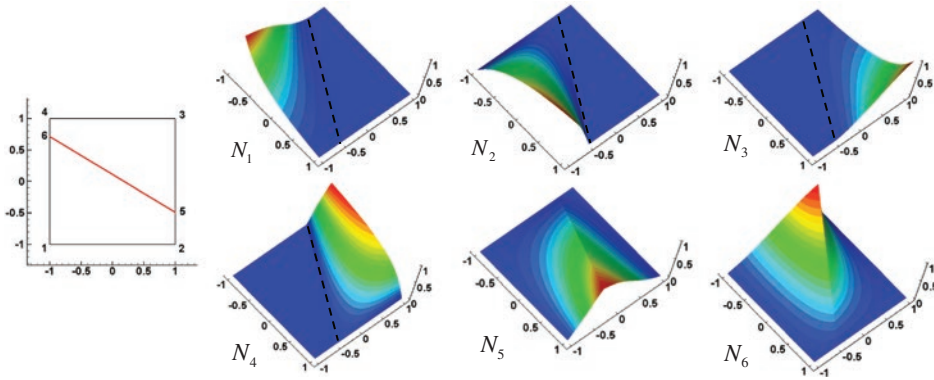


Figure 8. The basis functions of a four-noded quadratic element cut by an interface at the interior of two opposite edges.

An extension of the modified X-FEM was presented by Ventura et al. (2009) on the basis of a weighted X-FEM technique. The weighted X-FEM is similar to that proposed by Fries (2008), however – it introduces a general form based on multiplication of the standard enrichment function by a monotonically decreasing weight function with compact support. In this approach, a weight function, or a smooth function, $S(\mathbf{x})$ is constructed so that $S(\mathbf{x}) > 0$ only in the subdomain to be enriched. In fact, the approximation field (38) locally enriches the standard FEM approximation by $\psi_{\text{Mod}}(\mathbf{x})$, and locality is ensured by the compact support of $S(\mathbf{x})$. The enriched approximation field (38) based on the weighted X-FEM can therefore be written as:

$$\mathbf{u}^h(\mathbf{x}) = \sum_{I \in \mathcal{N}^{\text{std}}} N_I(\mathbf{x}) \bar{\mathbf{u}}_I + \sum_{I \in \mathcal{M}^{\text{enr}}} N_I(\mathbf{x}) S(\mathbf{x}) \psi(\mathbf{x}) \bar{\mathbf{a}}_I \quad (40)$$

and the shifted version of the enriched approximation field (40) can be defined as:

$$\mathbf{u}^h(\mathbf{x}) = \sum_{I \in \mathcal{N}^{\text{std}}} N_I(\mathbf{x}) \bar{\mathbf{u}}_I + \sum_{I \in \mathcal{M}^{\text{enr}}} N_I(\mathbf{x}) (S(\mathbf{x}) \psi(\mathbf{x}) - S(\mathbf{x}_I) \psi(\mathbf{x}_I)) \bar{\mathbf{a}}_I \quad (41)$$

In the weighted X-FEM, $S(\mathbf{x})$ is constructed using the polynomial ramp function that smoothes the transition from the enriched to unenriched elements. The non-enriched elements are those element with $S(\mathbf{x}) = 0$, and the enriched elements are those of $S(\mathbf{x}) \neq 0$. The graphical representation of the weighted function $S(\mathbf{x})$ and the modified function $R(\mathbf{x})$ are presented in Figure 7.

4.5. An alternative intrinsic enrichment method

In contrast to the standard X-FEM that uses a local extrinsic enrichment of the approximation space, an alternative method is introduced here for arbitrary

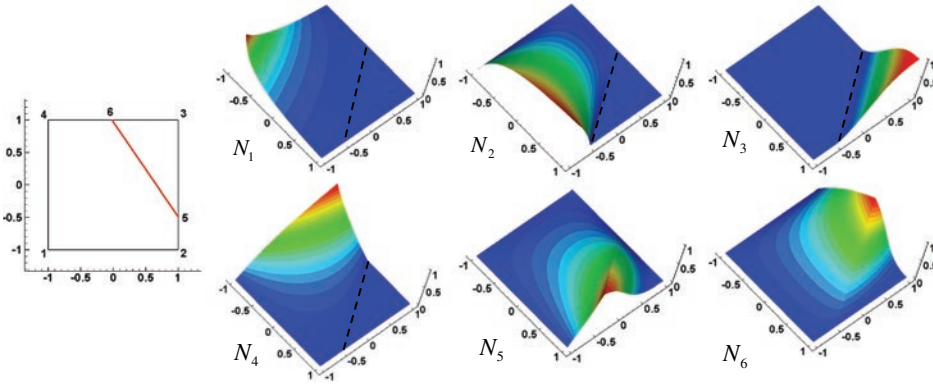


Figure 9. The basis functions of a four-noded quadratic element cut by an interface at the interior of two adjacent edges.

discontinuities based on an intrinsic enrichment strategy. The intrinsic enrichment is an idea to enhance the approximation space $\mathbf{u}^h(\mathbf{x})$ by including the new basis functions in order to capture a certain condition of complex field, such as discontinuity or singularity (Fries & Belytschko, 2006). In this method, the approximation space $\mathbf{u}^h(\mathbf{x})$ defined extrinsically in (14), and is enhanced intrinsically by establishing the new basis functions in order to capture the discontinuities as:

$$\mathbf{u}^h(\mathbf{x}) = \sum_{I \in \mathcal{M}} \hat{N}_I(\mathbf{x}) \bar{\mathbf{u}}_I \quad (42)$$

in which no extrinsic enrichment terms are introduced, and as a result no additional unknowns are involved. In the above relation, the basis functions $\hat{N}_I(\mathbf{x})$ are set to the standard FE shape functions in those parts of the domain where the polynomial approximation space is locally adequate, so $\mathcal{M} = 4$ for a four-noded bilinear element. However, in the vicinity of discontinuities, special basis functions are established so that they are able to capture discontinuities ($\mathcal{M} = 6$). In this technique, the basis functions $\hat{N}_I(\mathbf{x})$ are introduced implicitly by dividing an enriched element into two independent parts, and by defining the extra degrees of freedom at the intersection points of the interface and the edges of element. Hence, six basis functions $\hat{N}_I(\mathbf{x})$ are defined for a four-noded bilinear element cut by a discontinuity, as shown in Figures 8 and 9, in which $I = 1, 2, 3, 4$ refers to four nodal points of the element and $I = 5, 6$ refers to intersection points of the interface and the edges of element. In this technique, the basis functions are constructed by normalising the proper set of weight functions as:

$$\hat{N}_I(\mathbf{x}) = \mathcal{W}_I(\mathbf{x}) / \sum_{J=1}^6 \mathcal{W}_J(\mathbf{x}) \quad (43)$$

where $\mathcal{W}_I(\mathbf{x})$ denotes the weight function that reaches its maximum value at node I and vanishes along any side that does not include node I , defined as:

$$\mathcal{W}_I(\mathbf{x}) = \begin{cases} N_I(\mathbf{x})\psi(\mathbf{x})\frac{1}{2}(1 + \text{sign}(\varphi_I)\text{sign}(\varphi(\mathbf{x}))) & \text{for } I = 1, 2, 3, 4 \\ \hat{\psi}(\mathbf{x})\text{edge}(\mathbf{x}) & \text{for } I = 5, 6 \end{cases} \quad (44)$$

in which $N_I(\mathbf{x})$ are the standard shape function, and the absolute value of the level set function $\psi(\mathbf{x})$ and the modified enrichment function $\hat{\psi}(\mathbf{x})$ are respectively defined in (31) and (32). In the above definition, the edge function $\text{edge}(\mathbf{x})$ represents the position of an interface cut by the edges of an element, and has a zero value on one edge and unit value on opposite edge of bilinear element. In relation (44), the sign function $\text{sign}(\varphi(\mathbf{x}))$ is defined as:

$$\text{sign}(\varphi(\mathbf{x})) = \begin{cases} +1 & \varphi(\mathbf{x}) > 0 \\ -1 & \varphi(\mathbf{x}) < 0 \end{cases} \quad (45)$$

This function has the Kronecker-delta property with the zero value on opposite part of the element that produces independent displacements in two parts of an intersected element. In Figures 8 and 9, the basis functions of a four-noded bilinear element cut by an interface at the interior of two opposite edges, and also two adjacent edges are respectively presented. Obviously, the basis functions deal with independent deformations at both sides of intersected element by introducing the extra degrees of freedom at the intersection points of the interface and the edges of element.

5. Numerical simulation results

In order to illustrate the performance of proposed optimal X-FEM-type methods and to demonstrate a better understanding of their robustness in large deformation problems, three numerical examples with bimaterial weak discontinuities are presented. The examples are solved using the standard X-FEM, the X-FEM with modified enrichment function by Moës et al. (2003), the hierarchical X-FEM by Chessa et al. (2003), the corrected X-FEM technique by Fries (2008) and the intrinsic enrichment strategy proposed here. The first example is a plate with a circular hole at its centre under uniaxial tension chosen to demonstrate the performance of X-FEM for a benchmark linear bimaterial problem. In order to obtain the convergence rate of solution for various approaches, the energy norm of the numerical analysis is compared with that obtained from the analytical solution. The next example is a plate with a material interface at its centre chosen to illustrate the performance of various X-FEM approaches in a large plastic deformation problem. The last example is chosen to illustrate the performance of X-FEM technique in a practical engineering problem of the fibre reinforced composite. All three examples are simulated in a plane strain condition, and the acceptable tolerance of residual is set to 10^{-14} . The convergence analysis is performed for all three examples to investigate the accuracy and convergence rate of each approach.

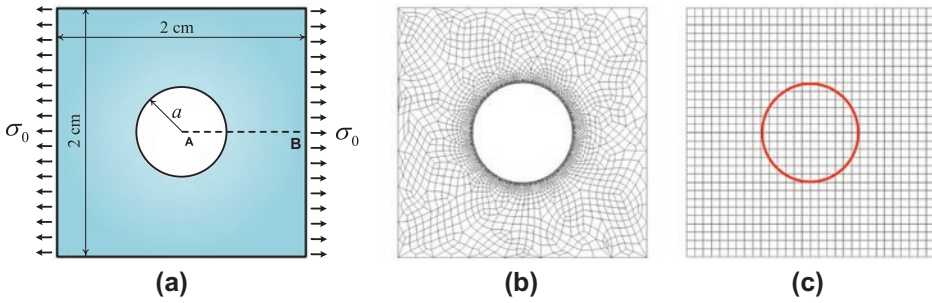


Figure 10. A plate with a circular hole at its centre; (a) problem definition, (b) the FEM mesh and (c) the X-FEM mesh of 30×30 elements.

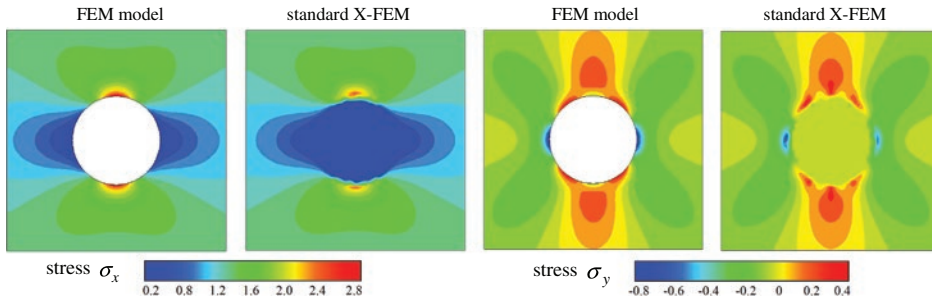


Figure 11. The distributions of stress σ_x and σ_y contours for a plate with a circular hole; a comparison between the FEM and standard X-FEM analyses.

In the first example, the X-FEM analysis is compared with the analytical solution, while for the next two examples, a very fine FE mesh is carried out as the reference solution to obtain the error of the energy norm. In large plasticity deformations, the error of energy is computed at each increment by:

$$e_S = \left(\int_{\Omega} (\Delta \mathbf{S}^* - \Delta \mathbf{S}^h)^T (\Delta \mathbf{E}^* - \Delta \mathbf{E}^h) d\Omega \right)^{1/2} \quad (46)$$

where $\Delta \mathbf{S}^*$ and $\Delta \mathbf{S}^h$ are accordingly the reference and X-FEM solutions of the incremental second Piola–Kirchhof stress field at the end of time step n , and $\Delta \mathbf{E}^*$ and $\Delta \mathbf{E}^h$ are correspondingly the reference and X-FEM solutions of the incremental Green strain field.

5.1. A plate with a circular hole at its centre

The first example is a plate with a traction-free circular hole at its centre which is subjected to a uniaxial tension, as shown in Figure 10. The analytical solution is available for this example as given by Szabó and Babuška (1991), and the X-FEM analysis was originally performed by Sukumar et al. (2001). In order to model the plate, the X-FEM analysis is carried out using a square plate of 2×2 cm with a

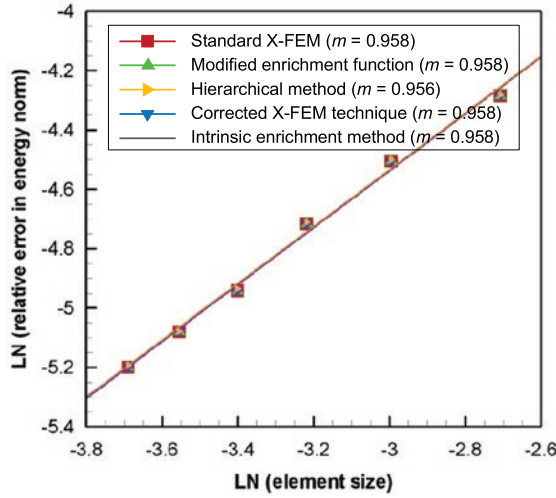


Figure 12. The error of the energy norm using various blending strategies for a plate with a circular hole.

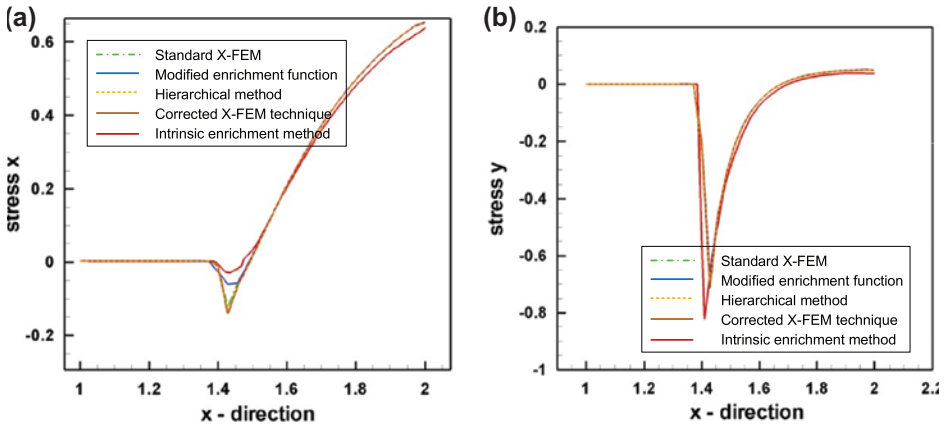


Figure 13. The evolutions of stress σ_x and σ_y along the centre line using various blending strategies for a plate with a circular hole.

circular hole of radius $a = .4$ cm at its centre. The plate is subjected to a uniform uniaxial tension of $\sigma_0 = 1$ kg/cm² along x -direction. In order to remove the rigid body modes, the exact tractions and appropriate constraints are imposed on the boundary of the plate. The material properties of the plate are as follows; the Young modulus of $E = 1 \times 10^5$ kg/cm² and the Poisson ratio of $\nu = .3$. In order to avoid singular stiffness matrices in the X-FEM analysis, the circular hole is assumed to be filled with a soft material as $E = 1 \times 10^2$ kg/cm².

The displacement fields of the plate can be obtained from the analytical solution in a polar coordinates system (r, θ) under a uniaxial tension of $\sigma_0 = 1$ kg/cm² as:

$$\begin{aligned}
 u(r, \theta) &= \frac{a}{8\mu} \left[\frac{r}{a}(\kappa + 1) \cos \theta + 2\frac{a}{r}((1 + \kappa) \cos \theta + \cos 3\theta) - 2\frac{a^3}{r^3} \cos 3\theta \right] \\
 v(r, \theta) &= \frac{a}{8\mu} \left[\frac{r}{a}(\kappa - 3) \sin \theta + 2\frac{a}{r}((1 - \kappa) \sin \theta + \sin 3\theta) - 2\frac{a^3}{r^3} \sin 3\theta \right] \quad (47)
 \end{aligned}$$

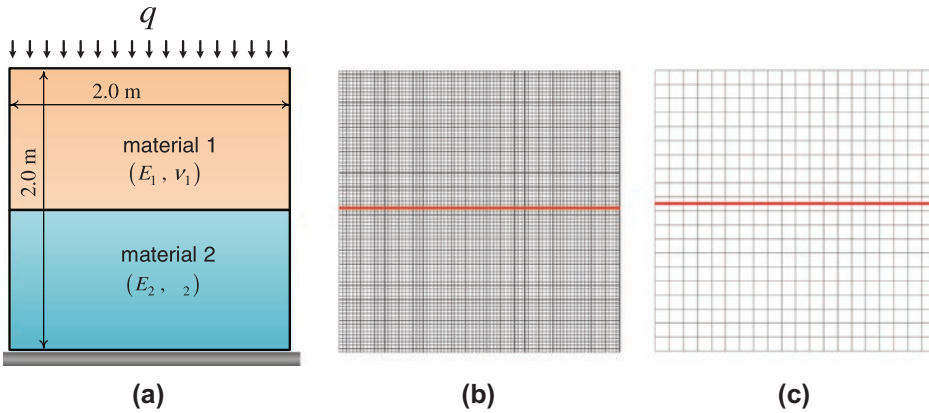


Figure 14. A plate with horizontal material interface; (a) problem definition, (b) the FEM mesh of 90×90 elements and (c) the X-FEM mesh of 20×20 elements.

where μ is the shear modulus, and κ is the Kolosov constant defined as $\kappa = 3 - 4\nu$ for plane strain and $\kappa = (3 - \nu)/(1 + \nu)$ for plane stress problems. The analytical stress components can be obtained as:

$$\begin{aligned}
 \sigma_x(r, \theta) &= \frac{1}{2} \left[1 - \frac{a^2}{r^2} + \left(1 - 4\frac{a^2}{r^2} + 3\frac{a^4}{r^4} \right) \cos 2\theta \right] \\
 \sigma_y(r, \theta) &= \frac{1}{2} \left[1 + \frac{a^2}{r^2} - \left(1 + 3\frac{a^4}{r^4} \right) \cos 2\theta \right] \\
 \tau_{xy}(r, \theta) &= \frac{1}{2} \left[-1 - 2\frac{a^2}{r^2} + 3\frac{a^4}{r^4} \right] \sin 2\theta
 \end{aligned} \tag{48}$$

In order to perform a convergence study, the X-FEM analyses are carried out using uniform structured meshes of 30×30 , 40×40 , 50×50 , 60×60 , 70×70 and 80×80 . In Figure 11, the distributions of stress contours σ_x and σ_y are presented for the FEM and standard X-FEM methods. Obviously, a reasonable agreement can be seen between two techniques. In Figure 12, the errors of the energy norm are plotted on a log-log plot using various blending strategies. This graph illustrates that the induced error is negligible and all approaches result in an optimal convergence rate. Obviously, all proposed approaches result in the same convergence rate for the plate with a circular hole at its centre in a linear small deformation problem. Finally, the evolutions of stress σ_x and σ_y along the horizontal line passing through the centre of the plate are plotted in Figure 13 for various blending strategies.

5.2. A plate with a horizontal material interface

The next example is chosen to illustrate the performance of various blending strategies for a large deformation problem of a plate with horizontal material interface subjected to a uniaxial compression, as shown in Figure 14. A square plate of 2×2 m is modelled in plane strain condition that is composed of two materials with the Young modulus of $E_1 = 1 \times 10^5$ kN/m² for the upper part

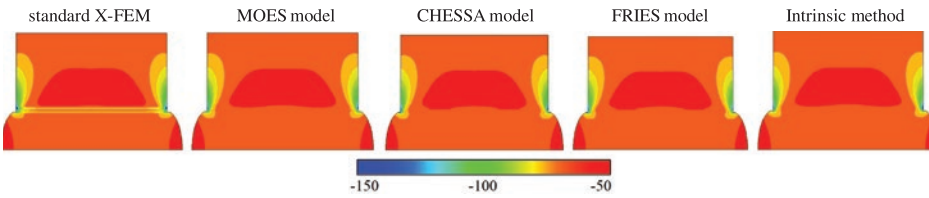


Figure 15. The distributions of stress σ_y contour for a plate with horizontal material interface; A comparison of the X-FEM technique with various blending strategies.

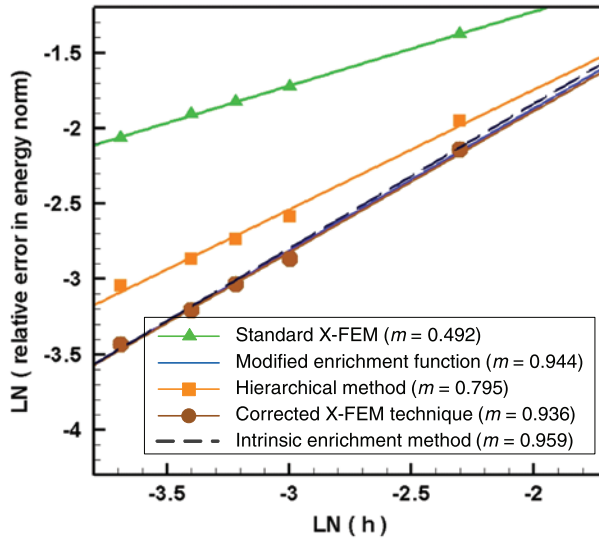


Figure 16. The error of the energy norm with various blending strategies for a plate with horizontal material interface.

and $E_2 = 1 \times 10^2 \text{ kN/m}^2$ for the lower part. The Poisson ratio is assumed to be the same for both materials as $\nu_1 = \nu_2 = .3$. The lower part of the component is assumed to have an elastoplastic von-Mises behaviour with the yield stress of 2400 kN/m^2 and a hardening parameter of $3 \times 10^4 \text{ kN/m}^2$, while the upper part is considered to have an elastic behaviour. The plate is restrained at the bottom edge and a uniform compaction with the intensity of $q = 55 \text{ kN/m}$ is applied at the top edge. A convergence study is carried out for this example by evaluation of the relative error of energy norm, and the rate of convergence is compared with an optimal convergence rate. To perform the convergence study, five uniform structured meshes of 20×20 , 40×40 , 50×50 , 60×60 and 80×80 are employed. Since the exact solution is not available for a comparison, a FE analysis with a fine mesh of 90×90 is carried out as a reference solution. In Figure 15, the distributions of stress σ_y contour are shown for the X-FEM technique with various blending strategies. Obviously, the effect of parasitic terms in the blending layer is obvious in the standard X-FEM while other approaches are in good agreement. In Figure 16, the errors of the energy norm are plotted on a log-log

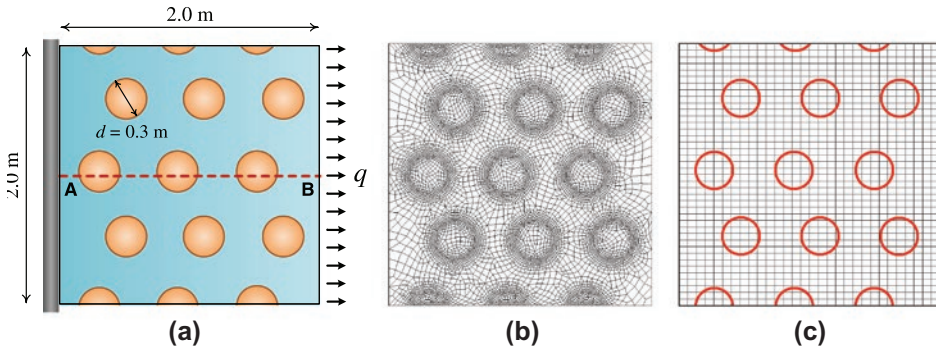


Figure 17. The fibre reinforced composite in uniaxial tension; (a) problem definition, (b) FEM mesh and (c) the X-FEM mesh of 40×40 elements.

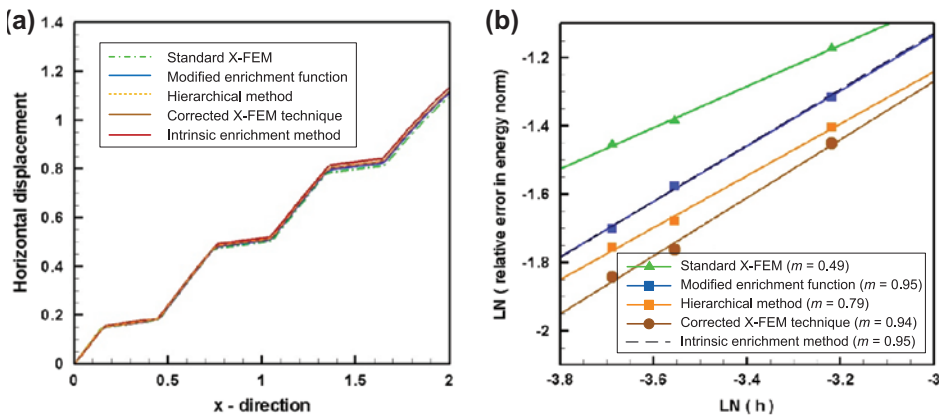


Figure 18. A fibre-reinforced composite in uniaxial tension, (a) the evolutions of displacement u_x along the line passing through the centre of the specimen and (b) the error of the energy norm using various blending strategies.

plot using various blending strategies. Remarkable improvement can be seen for all modified X-FEM techniques compared to the standard X-FEM with a suboptimal convergence rate of .492. It is noteworthy to highlight that while all proposed approaches result in almost optimum convergence rate, the hierarchical method presents a suboptimal convergence rate of .795. It must be highlighted that although the hierarchical method can be used to eliminate the parasitic terms in blending elements of polynomial order, it has two considerable weaknesses; the first is the insertion of extra DOFs that has to be costume tailored for every special problem, and the next one is that it is only suited for polynomial enrichments. It can be observed that the X-FEM with modified enrichment function introduced by Moës et al. (2003), the corrected X-FEM technique by Fries (2008), and the intrinsic enrichment strategy proposed here can be used efficiently to eliminate the parasitic effects and to achieve an optimum convergence rate in a large deformation problem.

5.3. The fibre-reinforced composite in uniaxial tension

In the last example, a practical engineering problem is investigated by modelling the fibre-reinforced composite in an uniaxial tension loading. The optimal X-FEM-type methods are carried out to illustrate the performance of various blending strategies in modelling of this complex geometry. In Figure 17, the geometry of a representative volume element is presented, where the circular fibres are distributed with random spatial distributions. It is assumed that the composite is made up of 20% volume of fibres embedded in an epoxy with no relative displacement on the interface of fibre and epoxy. In Figure 17(b) and (c), the FE mesh of the composite lamina is shown together with a typical structured mesh of linear quadrilateral elements used for the X-FEM analyses. A square plate of 2×2 m is assumed to have an elastoplastic von-Mises behaviour with the Young modulus of $E = 1 \times 10^4$ kN/m², Poisson ratio of $\nu = .3$, the yield stress of 2400 kN/m², and the hardening modulus of 3×10^4 kN/m². The plate is modelled in a plane strain condition that is reinforced with the circular fibres of radius $R = .15$ m, which have elastic behaviour with the Young modulus of $E = 1 \times 10^5$ kN/m² and Poisson ratio of $\nu = .3$. The plate is subjected to the uniaxial tension loading $q = 8 \times 10^3$ N/m.

A convergence study is carried out for this example by evaluation of the relative error of energy norm, and the rate of convergence is compared with the optimal convergence rate. To perform the convergence study, four uniform structured meshes of 40×40 , 50×50 , 70×70 and 80×80 are employed. Since the exact solution is not available for a comparison, a FE analysis with a fine mesh of 9134 elements is carried out as a reference solution. In Figure 18(a), the evolutions of displacement u_x are plotted for the mesh of 70×70 along the line passing through the centre of the specimen using various blending strategies. In Figure 18(b), the errors of the energy norm are plotted on a log-log plot using various blending strategies. Obviously, a suboptimal convergence rate of .49 can be seen from the standard X-FEM while other proposed approaches improve the convergence rate of the solution; however, the Hierarchical approach of Chessa et al. (2003) still presents a suboptimal convergence rate of .79. It can be highlighted that the X-FEM with modified enrichment function, the corrected X-FEM technique and the intrinsic enrichment strategy result in almost optimum convergence rate, while the corrected X-FEM technique can be used efficiently in a large plastic deformation problem.

6. Conclusion

In the present paper, the performance of blending elements in large plastic deformation with weak discontinuities was investigated employing several optimal X-FEM-type methods. The X-FEM formulation was presented in large plasticity deformations using a Lagrangian formulation. Several numerical examples were solved using the standard X-FEM, the X-FEM with modified enrichment function,

the hierarchical X-FEM and the corrected X-FEM technique, and the results were compared with an alternative intrinsic enrichment strategy proposed here. It was shown that the standard X-FEM results in a suboptimal convergence rate; although the hierarchical method removes the effect of parasitic terms in the blending layer, it presents still a suboptimal convergence rate; however the X-FEM with modified enrichment function, the corrected X-FEM technique and the intrinsic enrichment strategy can be used efficiently to achieve an optimum convergence rate, while the corrected X-FEM technique presents a great performance in large plastic deformation problems. Although the performance of various blending strategies in large plastic deformation has been studied here for two-dimensional problems, the above concluding remarks are valid for 3D cases, and can be efficiently applied within the 3D X-FEM computational algorithm for realistic industrial problems with any number of inclusions, however, it must be mentioned that an extension to 3D numerical simulation requires additional technical effort.

Acknowledgement

The first author is grateful for the research support of the Iran National Science Foundation (INSF).

Disclosure statement

No potential conflict of interest was reported by the authors.

References

- Belytschko, T., & Black, T. (1999). Elastic crack growth in finite elements with minimal remeshing. *International Journal for Numerical Methods in Engineering*, 45, 601–620.
- Belytschko, T., Black, T., Moës, N., Sukumar, N., & Usui, S. (2003). Structured extended finite element methods of solids defined by implicit surfaces. *International Journal for Numerical Methods in Engineering*, 56, 609–635.
- Bordas, S. P. A., Rabczuk, T., Nguyen-Xuan, H., Nguyen, V. P., Natarajan, S., Bog, T., ... Hiep, N. V. (2010). Strain smoothing in FEM and XFEM. *Computers & Structures*, 88, 1419–1443.
- Broumand, P., & Khoei, A. R. (2013). The extended finite element method for large deformation ductile fracture problems with a non-local damage–plasticity model. *Engineering Fracture Mechanics*, 112, 97–125.
- Chen, L., Rabczuk, T., Bordas, S. P. A., Liu, G. R., Zeng, K. Y., & Kerfriden, P. (2012). Extended finite element method with edge-based strain smoothing (ESm-XFEM) for linear elastic crack growth. *Computer Methods in Applied Mechanics and Engineering*, 209–212, 250–265.
- Chessa, J., Wang, H., & Belytschko, T. (2003). On the construction of blending elements for local partition of unity enriched finite elements. *International Journal for Numerical Methods in Engineering*, 57, 1015–1038.
- Fries, T. P. (2008). A corrected XFEM approximation without problems in blending elements. *International Journal for Numerical Methods in Engineering*, 75, 503–532.
- Fries, T. P., & Belytschko, T. (2006). The intrinsic XFEM: A method for arbitrary discontinuities without additional unknowns. *International Journal for Numerical Methods in Engineering*, 68, 1358–1385.

- Gracie, R., Wang, H., & Belytschko, T. (2008). Blending in the extended finite element method by discontinuous Galerkin and assumed strain methods. *International Journal for Numerical Methods in Engineering*, 74, 1645–1669.
- Gupta, V., Duarte, C. A., Babuška, I., & Banerjee, U. (2015). Stable GFEM (SGFEM): Improved conditioning and accuracy of GFEM/XFEM for three-dimensional fracture mechanics. *Computer Methods in Applied Mechanics and Engineering*, 289, 355–386.
- Khoei, A. R. (2005) *Computational plasticity in powder forming process*. Oxford, UK: Elsevier.
- Khoei, A. R. (2015). *Extended finite element method, theory and applications*. Sussex, UK: John Wiley.
- Khoei, A. R., Biabanaki, S. O. R., & Anahid, M. (2008). Extended finite element method for three-dimensional large plasticity deformations on arbitrary interfaces. *Computer Methods in Applied Mechanics and Engineering*, 197, 1100–1114.
- Khoei, A. R., Biabanaki, S. O. R., & Anahid, M. (2009). A Lagrangian-extended finite-element method in modeling large-plasticity deformations and contact problems. *International Journal of Mechanical Sciences*, 51, 384–401.
- Laborde, P., Pommier, J., Renard, Y., & Salaün, M. (2005). High-order extended finite element method for cracked domains. *International Journal for Numerical Methods in Engineering*, 64, 354–381.
- Loehnert, S., Mueller-Hoeppe, D. S., & Wriggers, P. (2011). 3D corrected XFEM approach and extension to finite deformation theory. *International Journal for Numerical Methods in Engineering*, 86, 431–452.
- Moës, N., Cloirec, M., Cartraud, P., & Remacle, J. F. (2003). A computational approach to handle complex microstructure geometries. *Computer Methods in Applied Mechanics and Engineering*, 192, 3163–3177.
- Natarajan S., Bordas S. P. A., Minh Q. D., Nguyen-Xuan H., Rabczuk T., Cahill L., McCarthy C. T. (2008). *The smoothed extended finite element method*. Proceedings of the 6th International Conference on Engineering Computational Technology, Greece.
- Nguyen-Xuan, H., Bordas, S. P. A., & Nguyen-Dang, H. (2007). Smooth finite element methods: Convergence, accuracy and properties. *International Journal for Numerical Methods in Engineering*, 74, 175–208.
- Shibanuma, K., & Utsunomiya, T. (2009). Reformulation of XFEM based on PUFEM for solving problem caused by blending elements. *Finite Elements in Analysis and Design*, 45, 806–816.
- Stazi, F. L., Budyn, E., Chessa, J., & Belytschko, T. (2003). An extended finite element method with higher-order elements for curved cracks. *Computational Mechanics*, 31, 38–48.
- Sukumar, N., Chopp, D. L., Moës, N., & Belytschko, T. (2001). Modeling holes and inclusions by level sets in the extended finite-element method. *Computer Methods in Applied Mechanics and Engineering*, 190, 6183–6200.
- Szabó, B., & Babuška, I. (1991). *Finite element analysis*. New York, NY: Wiley.
- Tarancón, J. E., Vercher, A., Giner, E., & Fuenmayor, F. J. (2009). Enhanced blending elements for XFEM applied to linear elastic fracture mechanics. *International Journal for Numerical Methods in Engineering*, 77, 126–148.
- Ventura, G., Gracie, R., & Belytschko, T. (2009). Fast integration and weight function blending in the extended finite element method. *International Journal for Numerical Methods in Engineering*, 77, 1–29.